International Journal of Geo-Information

MDPI

Article

A Technical and Operational Perspective on Quality Analysis of Stitching Images with Multi-Row Panorama and Multimedia Sources for Visualizing the Tourism Site of Onshore Wind Farm

Jhe-Syuan Lai, Yi-Hung Tsai, Min-Jhen Chang, Jun-Yi Huang and Chao-Ming Chi *

Department of Civil Engineering, Feng Chia University, Taichung 40724, Taiwan; jslai@fcu.edu.tw (J.-S.L.); d0610158@mail.fcu.edu.tw (Y.-H.T.); d0676303@mail.fcu.edu.tw (M.-J.C.); m0806485@mail.fcu.edu.tw (J.-Y.H.)
* Correspondence: cmchi@mail.fcu.edu.tw; Tel.: +886-4-2451725 (ext. 3120)

Abstract: A virtual tour of the onshore wind farm near Gaomei Wetland, Taichung City, Taiwan, was produced by producing panoramic images of the site by stitching images captured with a full-frame digital single-lens reflex camera and a multi-row panorama instrument, which automatically and precisely divided each scene into several images. Subsequently, the image stitching quality was improved by calculating the root mean square error (RMSE) of tie point matching and adjusting the tie points. Errors due to eccentricity attributed to the camera's relative position to the rotational axis of the multi-row panorama instrument were examined and solved; the effect of the overlap rate on image stitching quality was also investigated. According to the study results, the overlap rate between the original images was inversely proportional to the RMSE and directly proportional to the time required for photography and image processing. The stitching quality was improved by resolving eccentricity and by increasing the number of tie points. The RMSEs of the panoramas of all stations were all less than 5 pixels. Subsequently, multimedia materials providing information on wind turbine attributes were combined with the panorama platform to establish a virtual reality tour platform. The content of the platform could be accessed with a smartphone and viewed with a virtual reality device and could promote both tourist attractions and wind energy.

Keywords: green energy promotion; image stitching; multimedia; panorama; virtual tour

Citation: Lai, J.-S.; Tsai, Y.-H.; Chang, M.-J.; Huang, J.-Y.; Chi, C.-M. A Technical and Operational Perspective on Quality Analysis of Stitching Images with Multi-Row Panorama and Multimedia Sources for Visualizing the Tourism Site of Onshore Wind Farm. *ISPRS Int. J. Geo-Inf.* **2022**, *11*, 362. https://doi.org/10.3390/ijgi11070362

Academic Editor: Wolfgang Kainz

Received: 6 May 2022
Accepted: 23 June 2022
Published: 24 June 2022

1. Introduction

1.1. Challenge and Motivation

The global COVID-19 outbreak since November 2019 has severely disrupted everyday life. In response to the pandemic, businesses have established new models of interaction by incorporating virtual reality (VR) technology. Oscar et al. [1] proposed a virtual objective structured clinical examination (OSCE) method as an alternative learning option for students who could not participate in in-person examinations due to the pandemic. Gao et al. [2] developed a VR-based exercise platform to mitigate physical deterioration in people, particularly older adults, during COVID-19 quarantines, which prohibit outdoor activities. Van et al. [3] used VR to explore the role of human–machine interactive devices to revitalize the tourism industry in post-pandemic Vietnam.

1.2. Green Energies and the Tourism Site

With the increasing global focus on climate changes and sustainable development, renewable energy and green energy—such as solar, tidal, and particularly wind power—have garnered growing attention. Graabak and Korpås [4] suggested that wind power would be a primary source of power generation in Europe's future electricity system. According to Thayumanavan et al. [5], rapid development in power electronic converters over the past two decades has given wind power technology advantages over other renewable and green energy technologies, such as high power generation capacity, high conversion efficiency,

a pollution-free power generation process, and high availability. Studies on wind power development have been conducted in places such as Greece, China, and Taiwan [6–9]. This extensive research into wind power reveals its importance as a source of green energy. According to the Global Offshore Wind Speed Ranking report released by 4C Offshore, a market intelligence organization [10], 12 of the top 20 wind farms with the best wind conditions were located in the Taiwan Strait. The Taiwanese government plans to complete the development of 5.5 GW of offshore wind farms by 2025; moreover, they have implemented a series of policies promoting the development of industries related to onshore wind farms since 2000. Gaomei Wetland, located in Qingshui District, Taichung City, is a critical ecosystem conservation area and tourist attraction. Due to the proximity of the site to the large-scale onshore wind farms in the Port of Taichung, visualizing the site has excellent promotional value for both green energy and tourism.

1.3. Information-Technology-Based Visualizations

Due to technological advancements, information technologies and multimedia tools now facilitate incorporating sound, images, and text into VR. Burdea [11] proposed the three I's of VR—interaction, immersion, and imagination—that create a sense of presence for the user. Weng [12] proposed that people are the key factor for creating a sense of space and presence in a virtual space; changes in people's senses of space and presence prompt them to develop different perceptions in the space. VR has a wide range of applications. In education research, Bricken [13] reported that people exhibited a stronger motivation to learn in VR-based learning compared with conventional learning. Michitaka [14] discussed how virtual panoramas could be used to increase public interest in exhibitions and theaters. Lai et al. [15] employed VR and panoramic photography to establish a website for students to take a surveying practice course and reported that 92% of the study participants considered the website helpful to the course learning process. Studies on VR applications in engineering education, mechanical design, and physical education training [16–18] have verified the utility of VR in education. Regarding VR applications in tourism, the Louvre Museum provides VR panoramas of its interior to enable people to appreciate its paintings without visiting the museum in person [19]. A VR view of the Great Wall of China is publicly accessible on its official website [20]. Lee [21] established a three-dimensional virtual sightseeing platform of Taiwan's Yehliu Geopark to familiarize visitors with the park environment; 75% of the park visitors reported that the platform was helpful on a questionnaire survey. Harrington et al. [22] integrated data on the terrain, water, and plants in a botanical garden to design a realistic and immersive VR travel experience. Antonio et al. [23] employed the light detection and ranging (LIDAR) technology to digitally preserve historic sites in Cordova, Spain, and adopted VR technology to provide virtual tours of the sites. Other applications of VR in tourism include VR-based geoheritage tours in Iceland and icebreaking cruises in Hokkaido [24,25]; these VR projects enable those who cannot visit in person to immerse themselves in the experiences. Through a questionnaire survey and in-depth interviews, Chao [26] concluded that VR-based scientific experiments can expose people to events and objects that they would not otherwise experience in their everyday lives, thereby enhancing autonomous learning motivation. Li et al. [27] reported that VR increased tourist wellbeing and positively affected perceived value. Chiao et al. [28] examined the impact of virtual-tour-based platforms with different statistical indices (e.g., *p*-value and R-squared) for cultural tourism education. Given the aforementioned positive effects of VR in education and tourism, VR is an indispensable part of the evolution of the social model in response to the COVID-19 pandemic.

This study established a multimedia platform using panoramic technology due to its advanced development and low cost. In a panorama, the surrounding environment is presented in a cylindrical or spherical projection in VR space, providing the user with a 360° view of their position. In accordance with the approach proposed by [29], the 360° panoramas with a horizontal angle of 360° and a vertical angle of less than 180° were captured in this study. Panoramas are typically taken with one of two methods [15],

namely by using a 360° spherical camera to directly produce panoramas or by placing one or more cameras on a platform to capture images and stitching the images together. Compared with the second strategy, the first is simpler and more convenient but usually has a lower resolution and limited capability of customized functionality. The quality of image stitching in the second strategy is affected by the photography environment; for example, the production of high-quality images requires that the subject remains in the same position, that the subject's features are not overly monotonous, and that adequate lighting is present. These requirements are the main challenges in this strategy. The primary objectives of this study were to produce high-resolution panoramas and to offer customizable VR functionality. Therefore, the stitching strategy was employed. Ernie and Mark [30] suggested that capturing numerous images with high rates of overlap could facilitate producing high-resolution panoramas and that a 25% overlap is sufficient for generating 1-billion-pixel panoramas. Zheng et al. [31] detailed photography strategies and image stitching techniques. Liu et al. [32] improved the quality of image stitching through the use of extracting feature points and matching tie points. Lyu et al. [33] not only reviewed the pixel- and feature-based stitching methods for images, but also included video materials obtained from static and moving cameras. Lee et al. [34] proposed the improved optical flow algorithm to refine the task of image stitching.

1.4. Research Scopes

Accordingly, this study aimed to enable users to visit the Gaomei Wetland and the wind farm nearby the Port of Taichung virtually online and to understand the compositional structure and related information of wind turbines. First, multimedia visualization was performed on the onshore wind turbines; a low-cost, convenient process was developed that enables the user to view content by using a simple VR device (e.g., Google CARDBOARD) and clicking on a link or scanning a QR code, lowering the barrier to use for the system. From a technical perspective, two factors affecting the quality of high-resolution panoramic photography and image stitching are discussed: (1) the eccentricity effect attributable to the camera's relative position to the rotational axis of the panoramic instrument and (2) rates of overlap between images. The discussion could provide insight into the future development of VR technology, the promotion of tourist attractions and wind power, and the establishment of a panoramic visualization.

2. Materials and Methods

2.1. Study Area

Gaomei Wetlands, located to the south of the estuary of Dajia River, is a crucial ecosystem conservation area due to its expansive land area of 701.3 ha, rich natural resources, and status as one of the few places in Taiwan that is home to breeding colonies of *Anatidae* duck species. The wind farm near the Port of Taichung was dubbed "the wind turbine boulevard" due to the neat arrangement of its wind turbines along the flood-control road (Figure 1). An internationally renowned tourist destination, Gaomei Wetland attracts approximately 3.5 million tourists every year. The wind farm comprises 18 wind turbines manufactured by the Dutch company Zephyros. The total installed capacity is 2000 kW, composing 30% of the total capacity of the Taiwan Power Company Offshore Wind Farm Phase 1 Project. In sum, the site is critical for wind power generation in Taiwan.

2.2. Procedure

Figure 2 presents the research process. First, parameters on the panoramic instrument and camera were set and images were captured onsite. Subsequently, the overlapping images were stitched to produce panoramas, which were then imported to the proposed virtual tour platform. Next, a VR mode and other interactive functions were added to the platform to complete the panoramic visualization. The process is detailed in Sections 2.2.1 and 2.2.4. All image processing steps were performed on the Windows 10 (64-bit) computer

with Core i9-9900KF @ 3.60 GHz CPU, 32 GB RAM, and NVIDIA GeForce RTX 2080 GPU (graphics size: 8010 MB).

(**A**)

(**B**)

(**C**)

Figure 1. Study site (**A**) in Taichung, Taiwan (**B**) and onshore wind farms (**C**).

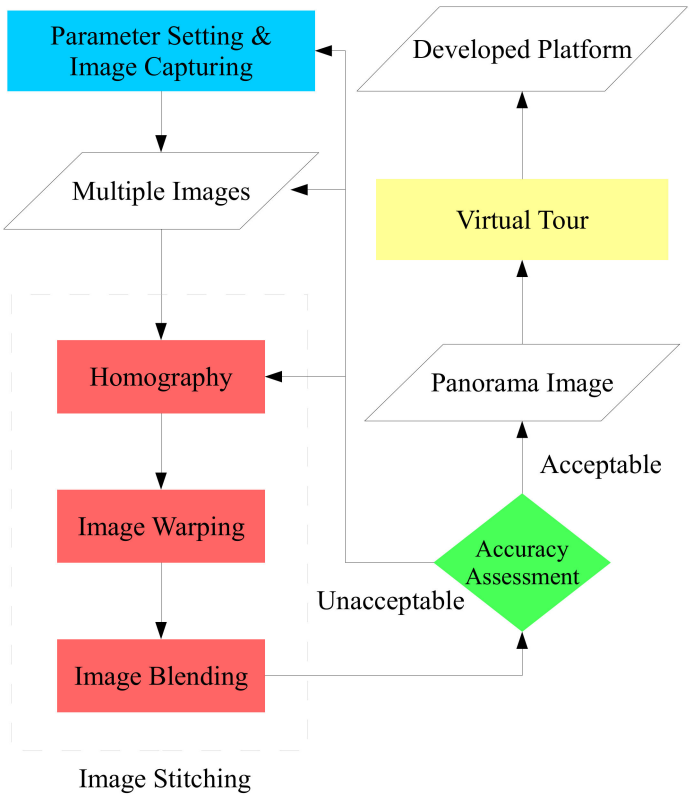

Figure 2. Study procedure (each color will be presented in the same section).

2.2.1. Parameter Setting and Image Capturing

The GigaPan EPIC Pro V panorama device (hereafter "GigaPan"), which produces multi-row panoramas (Figure 3), and Canon EOS 6D Mark II camera equipped with the Canon EF 16–35 mm F/4L IS USM, an ultra-wide-angle zoom lens, were used for panoramic photography. A test shoot was performed in Feng Chia University, Taichung City, before the panoramic photography at the wind turbine boulevard. The test shoot was performed to test the parameter settings and to use the panoramic instrument to control the overlap rate to calculate the root mean square error (RMSE) after tie point stitching. The test shoot results served as a basis for the parameter settings used at the actual shoot at the wind turbine boulevard. GigaPan offers a range of shooting modes; the 360 Panorama mode selected in this study requires the user to set the upper and lower image limits and the number of images captured from each angle before connecting to the camera for automatic 360° panoramic photography. In this mode, the instrument rotates automatically and precisely divides a scene into several grid images. The camera was set to manual mode, and its parameters were adjusted to obtain the optimal parameter combination for the environment. The exposure value was set to bracketing mode and three shots—bright, normal, and dark—were taken with the camera from each angle. An optimal image from the three shots was then selected for stitching.

For cameras to adapt quickly to various environmental and brightness conditions, several exposure control modes have been developed since the development of microelectronic technology in the 1980s [35]. In this study, the manual mode was adopted in which all shooting parameters are set by the user, including the aperture size and shutter speed. For this study, the parameters were set in accordance with the study area's bright, outdoor environment and the constantly changing external factors (e.g., clouds or other moving objects). The camera aperture size, in addition to its basic function of regulating the amount of light passing through the lens, can also be adjusted to improve image quality and control the depth of field. A large aperture size enables the camera to capture details in a short time (high shutter speed) assuming that adequate lighting is present. With a small aperture

size, the camera takes longer (low shutter speed) to capture the scene. Shutter speed is a critical component that controls the length of time that light can pass through the lens and determines the camera's ability to freeze a moving object. Moreover, shutter speed controls the amount of light to which the image sensor is exposed and can be used to minimize the effect of camera vibrations on images, preventing unwanted movements or blurs from appearing in the images [36]. Shutter speed directly affects the brightness of an image; a lower shutter speed causes the camera to capture more reflected light or light sources. If lighting is sufficient, a higher shutter speed enables the camera to capture more subject details. ISO represents the sensitivity of the camera to light, and the ISO setting must be adjusted particularly carefully because an overly high ISO results in grainy images and blurs the image content. This is because a high ISO enlarges the electronic signals and creates noise. To minimize noise, the photographer must determine the optimal ISO value based on their experience and repeated testing.

(**A**) (**B**)

Figure 3. Panoramic instrument of GigaPan EPIC Pro V. (**A**) Eccentric issue caused by different axes of rotation between panoramic instrument (red part) and camera (blue part); (**B**) Adjustable position (scale marks) to put camera (red part).

In addition, the rate of image overlap controlled by GigaPan affects the quality of image stitching. A high overlap rate requires more images to be captured in both the vertical and horizontal directions, which facilitates the extraction of feature points in the overlapping areas and the matching of these points as tie points. Therefore, a high overlap rate improves the quality of image stitching, but requires increased time for shooting and image processing. Conversely, a low overlap rate requires a short shooting time but has low stitching quality; to improve the quality, the tie point positions must be adjusted manually. Therefore, the overlap rate is correlated positively to the shooting time, image processing time, and number of tie points and negatively to labor cost. Assuming that image stitching quality must be high, a trade-off exists between the overlap rate and labor cost. The geometrical relationship between the rotational axes of the image center and GigaPan is also a variable. If the perpendicular axes of these two rotational axes are not in the same axial direction (Figure 3A), eccentricity may occur, which causes the actual overlap rate to deviate from the GigaPan's overlap rate setting, thus reducing the stitching quality. In this study, an eccentric calibrated field was established; the camera's position was adjusted in accordance with the scale on GigaPan (Figure 3B) to compile a look-up table for focal length. Figure 4A presents the eccentric calibrated field; the camera, benchmark rod, and the center of the benchmark paper form a straight line. Lengths I and II are of the same length. Images were captured with the camera with the GigaPan rotated to determine whether the benchmark rod completely overlaps with the axis perpendicular to the benchmark paper center in the images to determine whether eccentricity was present. Eccentricity

did not exist if the benchmark rod and the axis perpendicular to the benchmark paper center remained completely overlapped as the GigaPan rotated right or left (Figure 4B). Figure 4C,D depicts images demonstrating the presence of eccentricity. If the benchmark rod shifted to the left or right when GigaPan rotated rightward or leftward, respectively, the camera should be moved to a greater mark value on the scale. Conversely, if the benchmark rod shifted to the right or left when GigaPan rotated rightward or leftward, respectively, the camera should be moved to a smaller mark value on the scale.

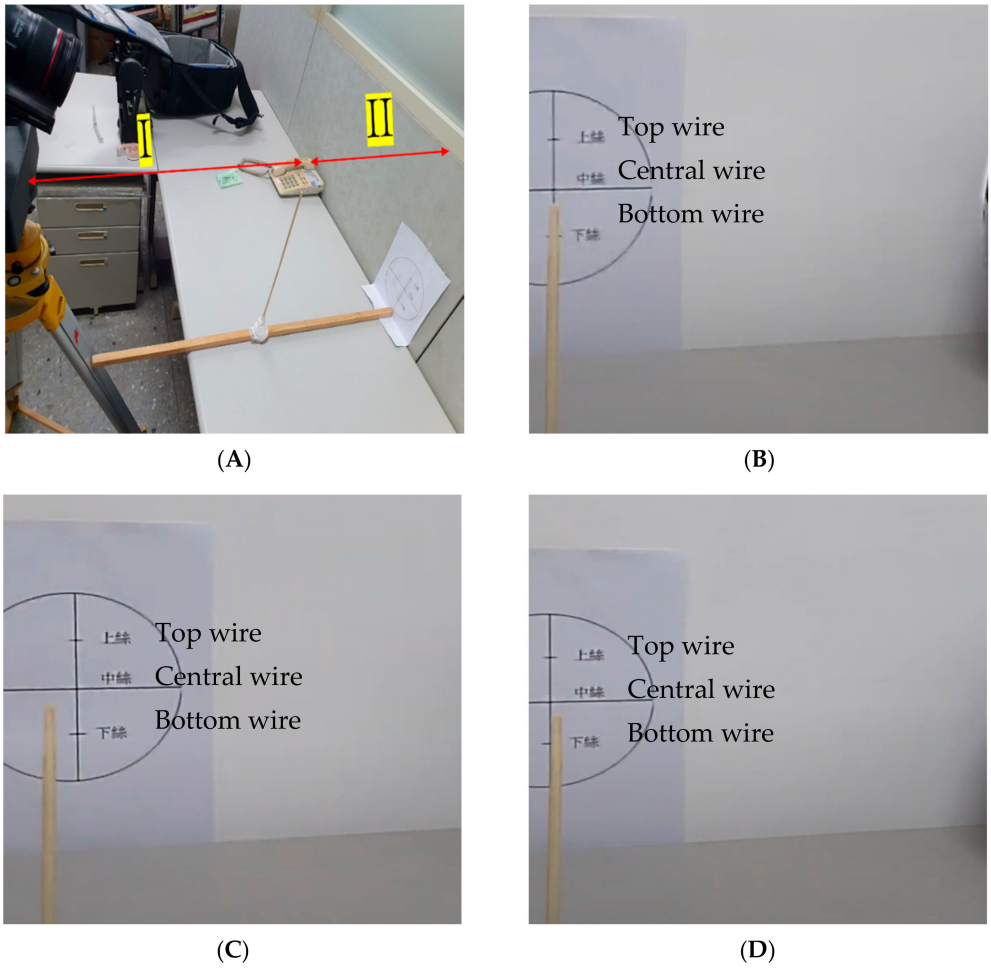

Figure 4. Developed field for calibration of eccentric issue between camera and panoramic instrument. (**A**) Calibrated field; (**B**) Non-eccentric issue; (**C**) Eccentric issue with left shift; (**D**) Eccentric issue with right shift.

2.2.2. Image Stitching

After the completion of a fixed-point shoot, the individual captured images were stitched into a panorama by using Kolor Autopano Giga version 4.4 (hereafter "Autopano"). The image stitching procedure is marked with a dotted box in Figure 2. Stereoscopy was employed for photography in this study; feature points were extracted from images captured from different angles. Image matching was performed to identify pairs of feature points and subsequently create tie points. Capturing numerous images with a high overlap rate, despite the required long image processing time, provides many tie points and thus improves the image stitching quality. Subsequently, the stitched images were rendered to remove motion trails (e.g., of wind turbine blades or people) to simplify the subsequent image-editing procedure. Image stitching comprises three stages: homography, warping, and blending; these are detailed in the following text.

- Homography

Homography involves the transformation of two images captured from different angles by identifying corresponding feature points in the same plane and the overlapping areas between the images. Autopano was used for image stitching; the algorithm employs a scale-invariant feature transform (SIFT) to reduce the effects of image rotation, scale, and grayscale value differences on feature points in image pairs [37], thus facilitating the extraction and matching of feature points for tie point generation. Subsequently, homogeneous coordinates were used to obtain a 3 × 3 matrix h to document the image translation, scaling, and rotation in different spaces as a preparation for subsequent steps. For example, if the feature point set of one image is $(x, y, 1)$, and that of another is $(x', y', 1)$, the mapping relationship between the tie points of the two images can be presented as a 3 × 3 matrix h as in Equation (1).

$$\begin{bmatrix} x \\ y \\ 1 \end{bmatrix} = \begin{bmatrix} h_{00} & h_{01} & h_{02} \\ h_{10} & h_{11} & h_{12} \\ h_{20} & h_{21} & h_{22} \end{bmatrix} \times \begin{bmatrix} x\prime \\ y\prime \\ 1 \end{bmatrix} \quad (1)$$

The establishment of the transformation matrix H between the two images requires determining the relationships between four pairs of feature points in the two images [38]. However, because more than four feature point pairs between two images are typically identified, the optimal pairs—those with the least error—should be used. Autopano employs the random sample consensus (RANSAC) algorithm to remove outliers [31]. In the algorithm, a random subset of the population of numerical values is selected to estimate the optimal model parameters. The numerical values comprise inliers that conform to the numerical model and outliers that do not fit the model. The outliers are detected by the suggested threshold of Autopano in this study. Different inlier points are substituted into Equation (1) to determine the set of inliers with the least error (the optimal solutions).

- Image Warping

According to homography calculations, the identification of corresponding tie points requires the use of homogenous coordinates for determining the level of image distortion in the space in the subsequent image warping step. For example, to stitch two images, one image is used as the reference image, and the other is projected through algorithmic computations and warping, onto the coordinate space of the reference image to ultimately superimpose the two images. The projection procedure, comprising forward and backward warping, involves determining the positions of target pixels in the space before placing the original image pixels over the target image. Subsequently, repeated calculations are conducted by using an inverse function to restore damages in the forward warped image. Distortion that often occurs in the non-overlapping areas of the image during projection can be effectively reduced using cylindrical and spherical projections.

In this study, a spherical projection was used to produce 360° panoramas without excessive image distortion. Equation (2) is the transformation between spherical and Cartesian coordinate systems. Given an image coordinate (x, y) and its projection on a spherical surface (x, y, f), the spherical coordinate is presented as (r, θ, φ), where r represents the distance from the center of the sphere and the target, θ is the angle between r and the zenith with a range of $[0, \pi]$, and φ is the angle between the planar projection line of r and the x-axis with a range of $[0, 2\pi]$.

$$(r \sin\theta \cos\varphi, r \sin\theta \sin\varphi, r \cos\theta) \propto (x, y, f) \quad (2)$$

- Blending

Image blending is the last step of image stitching. Various image blending methods have been proposed, including feather blending and multi-band blending. The purpose of blending is to synthesize the warped images to create a gradient effect in the overlapping area of the two images. By using color balancing algorithms, multiple images can be modified to look like a single image. There is no general consensus at present as to which is

the best blending method to apply. It is subjective, as well as depending on purpose. This process is further detailed in [39–41].

2.2.3. Accuracy Assessment

To produce panoramas, Autopano presents the RMSE of tie points in each panorama to demonstrate its stitching quality. RMSE is a common measure of numerical differences and is often used to evaluate model predictions or observed estimates. A root mean square deviation indicates an error between the predicted and observed values (i.e., the presence of sample standard deviation). An error derived from a sample-based estimation is often known as residual error. In the context of panoramas, RMSE is defined as in Equation (3), where N denotes the number of tie points, and $Diff$ is the pixel displacement between matched tie points.

$$\text{RMSE} = \sqrt{\frac{\sum_{i=1}^{N} Diff_i^2}{N}} \quad (3)$$

RMSE, calculated using the pixel distance between tie points after image warping, is highly sensitive to excessively large or small errors in a group of measurements and thus effectively reflects the preciseness of measurements [42]. In this study, the quality of image stitching was evaluated with the RMSE color index, which was calculated using Equation (3). The index value offers a precise indication of the image stitching quality for users to plan a subsequent image processing procedure. In this study, an index value of less than 5 pixels indicates good image stitching quality; larger and smaller values indicate lower and higher quality, respectively. Image stitching quality was determined entirely on the basis of numerical values without naked-eye evaluations.

2.2.4. Virtual Tour

Overlapping original images were stitched into panoramas in Autopano; these were then imported to the Kolor Panotour version 2.5.8 (hereafter "Panotour") platform to establish a virtual tour environment. The platform was customized by adding relevant attributes and multimedia materials, including videos, menus, and audio navigation. Next, the platform was exported as a webpage, and its address was converted into a QR code. Users could visit the webpage simply by scanning the QR code on their phone and access the established VR environment with a VR headset for tourism purposes and improving learning outcomes. Koehl and Brigand detailed the functions and applications of Autopano in [43].

3. Results

3.1. Camera Settings

Daylight during our shoot was sufficient; thus, the aperture size was set to F/8–F/11. Because the strong wind at the wind farm caused camera shake, which may result in blurry images, the shutter was set to high speeds throughout the shoot, apart from some slight adjustments to compensate for the lighting conditions; for example, the shutter speed was set at 1/300 when a large aperture size was used. Given the sufficient daylight, ISO was set between 100 and 200.

3.2. Test for Eccentric Issue and Rate of Overlap

The Canon EF24–70 mm F/2.8L II USM was used for the shoot. Table 1 presents the relationship between the camera's focal length and its position (presented using the scale mark on GigaPan), which was determined according to the calibrated field displayed in Figure 4A. Because the calibrated field was located in an indoor space, the ISO, aperture size, and shutter speed were set at 800, F10, and 1/30, respectively. Table 1 reveals that the optimal scale mark value varied across focal lengths. Specifically, the optimal scale mark values for the 24, 35, and 70 mm focal lengths were 105, 100, and 80, respectively. If the camera was placed at a smaller scale mark value, the benchmark rod in the captured image

would shift to the left in the clockwise rotation of GigaPan; if the camera was placed at a larger scale mark value, the benchmark rod in the image would shift to the right.

Table 1. Look-up table for eccentric issue with different focal lengths (bold indicates the suggested scale marks).

24 mm		35 mm		70 mm	
Scale Mark	**Object Shift in Clockwise**	**Scale Mark**	**Object Shift in Clockwise**	**Scale Mark**	**Object Shift in Clockwise**
30	left	30	left	30	left
55	left	55	left	55	left
100	left	**100**	-	**80**	-
105	-	115	right	100	right
110	right				
115	right				

The effects of focal length, scale mark, and overlap rate on stitching quality were further investigated. A test shoot was conducted at the square outside the Science and Aeronautical Engineering Building of Feng Chia University by using 27 combinations of focal length, scale mark, and overlap rate. Two levels of overlap rate for the half-sampling were considered, i.e., Level 1 (50%) and Level 2 (25% and 75%). Thus, three overlap rates (25% (low), 50% (moderate), and 75% (high)) and two focal lengths (24 and 35 mm) were used. Table 2 presents the stitching error obtained using these parameter combinations; RMSE represents the average RMSE of all tie point stitching in a single panorama. With the 24 mm focal length, the stitching quality was the highest at scale mark 105 for all overlap rates, and the RMSE was 2.56 for the 25% overlap rate, 2.45 for the 50% overlap rate, and 2.15 for the 75% overlap rate. If the focal length was 35 mm and the scale mark value was 100, the RMSE was 2.56 for the 25% overlap rate, 2.69 for the 50% overlap, and 2.15 for the 75% overlap. In addition, the camera's optical center was the farthest from the rotational axis of GigaPan when the scale mark value was 55 or 33 with a focal length of 24 or 35 mm, respectively, which resulted in the highest RMSE and thus the poorest stitching quality. The test shoot results (Table 2) were in agreement with the recommended scale mark positions in Table 1. Accordingly, the presence of eccentricity was strongly negatively associated with the quality of panorama stitching. Regarding processing loading, the duration of the (1) capturing time, (2) degree of stitching period, and (3) number of images with different overlap rates is 3 min, short, and 60 for 25%, 6 min, middle, and 105 for 50%, and 16 min, long, and 273 for 75%, respectively.

Table 2. Quality analysis with different rate of overlap and scale marks (bold indicates the suggested scale marks).

24 mm			35 mm		
Rate of Overlap	**Scale Mark**	**Avg. RMSE (Unit: Px)**	**Rate of Overlap**	**Scale Mark**	**Avg. RMSE (Unit: Px)**
25%	55	2.82	25%	30	2.96
	100	2.74		55	2.89
	105	**2.65**		**100**	**2.56**
	110	2.87		115	2.74
	115	2.75			
50%	55	2.72	50%	30	2.87
	100	2.56		55	2.82
	105	**2.45**		**100**	**2.69**
	110	2.55		115	2.69
	115	2.70			
75%	55	2.51	75%	30	2.47
	100	2.26		55	2.45
	105	**2.15**		**100**	**2.21**
	110	2.19		115	2.27
	115	2.22			

Figure 5 visualizes the stitching results with a focal length of 24 mm, an overlap rate of 25%, and scale mark values of 10, 55, and 105. Table 3 presents the numbers of tie points and average RMSEs. Figure 5A presents the panorama; Figure 5B–D shows zoomed views of the area marked by the red box in panoramas produced using different scale mark values for a comparison of the stitching quality and to verify the effect of the scale mark position on the stitching result. Figure 5B,C has displacement and blurs, whereas the result in Figure 5D is clear and superior. The test shoot results (Table 2 and Figure 5) obtained using recommended scale mark positions in Table 1 reveal that the number of tie points was positively correlated with stitching quality and that greater eccentricity was associated with a larger RMSE.

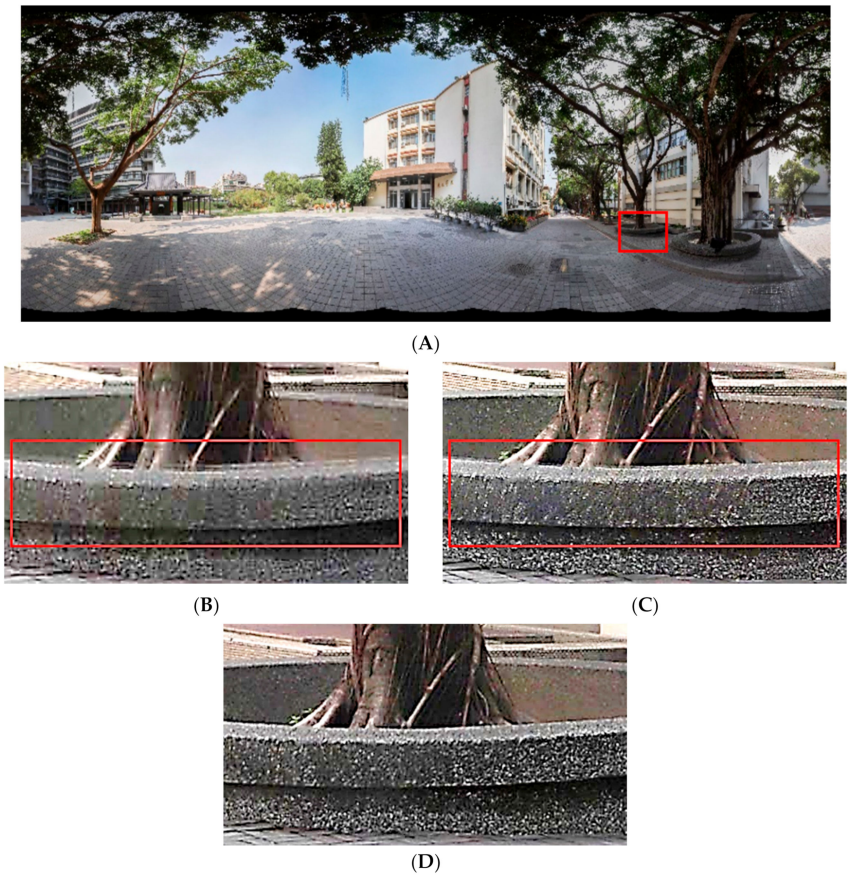

Figure 5. Visualizing the stitched errors for 25% of overlap with different scale marks. (**A**) Stitched image and area of interest (red part) for comparison; (**B**) Zoom-in (**A**)'s red part with the case of scale mark 10; (**C**) Zoom-in (**A**)'s red part with the case of scale mark 55; (**D**) Zoom-in (**A**)'s red part with the case of scale mark 105.

Table 3. Comparison between number of tie points and avg. RMSEs with different scale marks.

Rate of Overlap	Scale Mark	Number of Tie Points	Avg. RMSE (Unit: Px)
25%	55	161	2.82
	105	**194**	**2.65**
	115	166	2.75

3.3. Real Case of the Onshore Wind Farms

Images were captured from top to bottom and left to right; each image had a 50% overlap with its adjoining images. The scale mark at which the camera was placed was determined in accordance with Table 1. Feature points were extracted from the overlapping

area and subsequently matched into tie points for image stitching. When stitching was complete for panoramas, Autopano presents the stitching quality of each tie point in colors (Figure 6). Green indicates an RMSE of less than 5 pixels (high-quality stitching); orange represents an RMSE of between 5 and 10 pixels (moderate quality); and red denotes an RMSE greater than 10 pixels, indicating that the tie point be adjusted or removed. If the photography subject is glass, a surface with a solid color, or an object lacking distinct features, the photograph lacks feature points for extraction, resulting in few or even incorrect tie points. Consequently, human intervention may be necessary to adjust and add new tie points. We drag-selected incorrectly matched tie points to correct them, extracted new feature points, or stitched unmatched parts together until all stitches were of high quality (green). If the modification was complete, the images were rendered to reduce or remove motion trails and blurs and output the final complete panoramas. The panoramas were then imported into Panotour for functional customization.

Figure 6. Quality illustration of tie points (left) and the edited interface (right) in Autopano after stitching a panoramic image.

Figure 7 presents the locations at which the panoramas were captured. The shoot began at Station A and continued along the wind turbine boulevard to Station F for a total of six stations. The stitching quality obtained at each stop and the corresponding panoramas are presented in Table 4 and Figure 8, respectively. According to Table 4, Station A (Figure 8A) had the smallest RMSE standard deviation; that is, the stitching quality remained similar across the entire panorama compared with those of other stations; however, the average RMSE was higher than at other stations. Stations C and D (Figure 8C,D) had the lowest average RMSEs, indicating that their panoramas had the highest overall stitching quality among all stations. Moreover, the number of tie points was proportional to the stitching quality and inversely proportional to RMSE; therefore, increasing the number of tie points could effectively improve stitching quality. The number of tie points was also associated with the weather and the number of features on the subject at the shooting site. According to the RMSE classification of Autopano, all panoramas produced in this study were of high quality, and all of their RMSEs satisfied the basic requirement (less than five pixels) after manual correction.

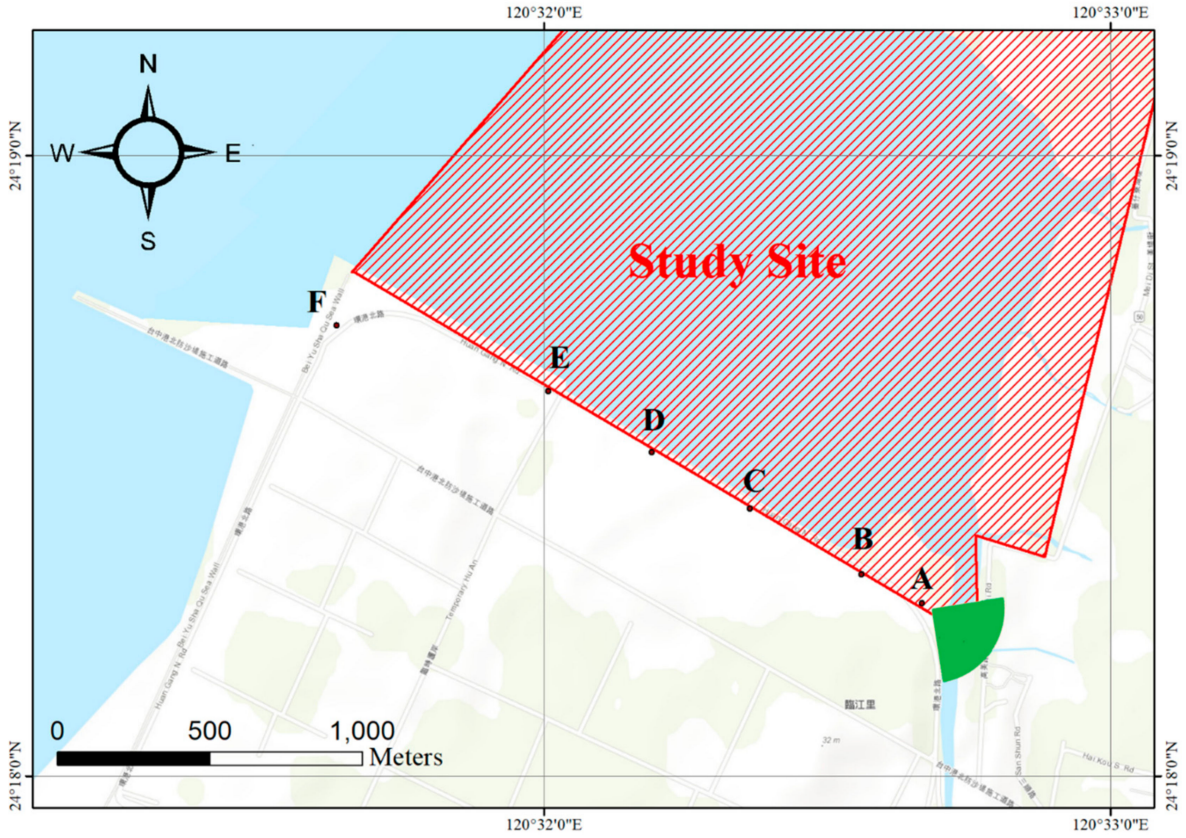

Figure 7. Locations of panoramic stations (points indicate panoramic stations, and the green symbol represents user's current field of view).

Table 4. Statistics of RMSEs with different stations (unit: pixel).

Station	Sd.	Avg.	Max	Min	Number of Tie Point
A	0.50	3.36	4.59	2.10	171
B	0.95	3.04	5.62	1.33	238
C	0.72	2.65	5.74	1.39	366
D	0.56	2.65	5.11	1.65	355
E	0.64	2.78	5.28	1.50	393
F	0.52	3.24	4.58	1.94	155

(**A**)

Figure 8. *Cont.*

(**B**)

(**C**)

(**D**)

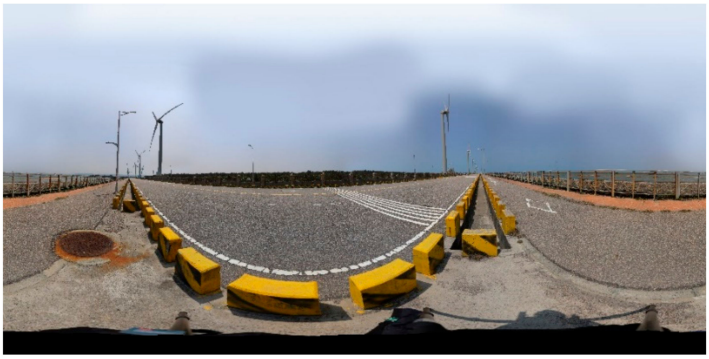

(**E**)

Figure 8. *Cont*.

(**F**)

Figure 8. Stitched images station by station. (**A**–**F**) indicate Stations A to F, as shown in Figure 7.

The panoramas for all stations were stitched in Autopano (Figure 8) before being imported to Panotour to establish the virtual tour platform. To ensure that users could engage in a travel experience at any time and could learn from their experience with multimedia technologies without being interrupted by external factors, the platform design was begun by considering the compositional structure of and relevant information regarding wind turbines. The platform (Figure 9) was designed with various functions using Panotour. The relationship among the stations was set in accordance with the tour route for learning purposes during the tour. When users enter the developed environment of a station, they first listen to a spoken commentary, such as an introduction to the history of the Gaomei wind turbine boulevard or navigation instructions for the platform. The audio ends with the sound of wind turbine operation to enhance the authenticity of the virtual tour. The green arrow in Figure 9 is a connector that leads to the panorama of the next station; these arrows enable users to virtually visit the stations one by one as if they were actually walking along the wind turbine boulevard. With a simple VR headset, users can view the VR environment simply by clicking on VR mode in the control bar and visiting the website on their phones (Figure 9F). However, the field of vision is fixed, capturing from the six panoramic stations (Stations A to F). Participants can only browse at a horizontal angle of 360° from these panoramic stations. If participants want to move to other stations, there are two approaches. First is to click the connectors (e.g., green arrows in Figure 9), or to click the point in Figure 7. After that, the field of view (i.e., the green area in Figure 7) will be changed by the user instantaneously.

(**A**)

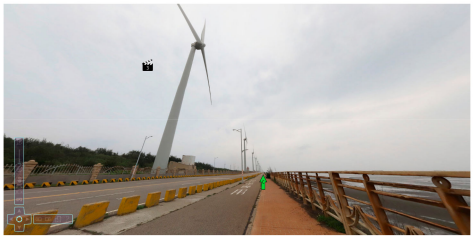

(**B**)

(**C**)

(**D**)

Figure 9. *Cont.*

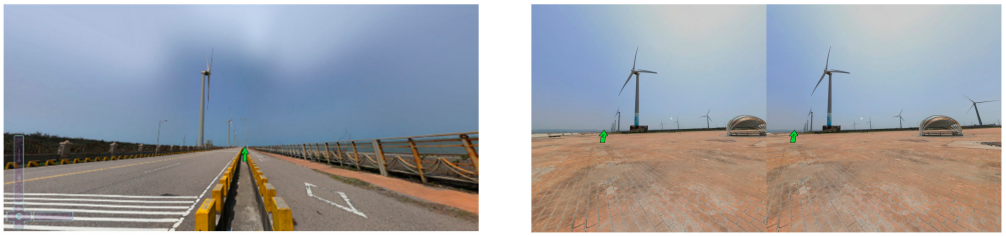

(**E**) (**F**)

Figure 9. Scenes in the developed virtual tour environment with the connectors for browsing multiple panoramic stations. (**A**–**F**) indicates Stations A to F, and (**F**) shows the VR mode.

Figure 10 presents the scene for the main station (Station A). Interacting with Symbol 1 brings users to an introduction of the wind turbine attributes, including the manufacturer, type of power generator, model, installed capacity, diameter of blade, and total weight; this introduction serves to provide an overview of the wind turbines at the park (Figure 11). Symbol 2 is a button that activates an education video illustrating a wind turbine concept; one illustration video was prepared for each of the five stations (Table 5). The video for Station A presents the operation of a wind turbine; that for Station B details the transportation of electricity; that for Station C describes the construction of the gravity-based foundation; that for Station D provides an overview of wind turbine construction and electricity transportation; and that for Station E introduces the monopile foundation for offshore wind turbines. These videos served to familiarize users with the principles involved in the construction and operation of wind turbines (Figure 12). Symbol 3 in Figure 10 presents the control bar with which users can adjust the zoom level, travel to the previous or next station, or turn on the VR mode. Symbol 4 is a mini map that tells users their current position and the direction they are heading along the tour route; users can also click on a station icon to travel to a particular station. The cross mark in the VR headset, pointing (few seconds) the connectors for browsing multiple panoramic stations (e.g., green arrows in Figure 9) and videos (e.g., Symbol 2 in Figure 10), can be able to interact with these customized functions.

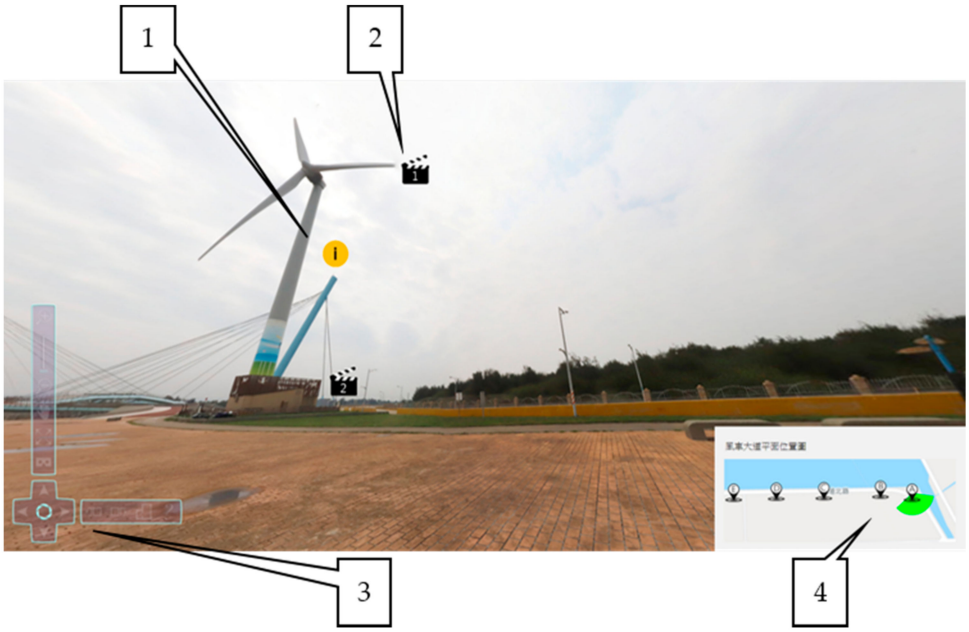

Figure 10. Main station (Station A) of the developed virtual tour environment. Symbol 1: more information, Symbol 2: video for illustration, Symbol 3: control bar, Symbol 4: guide map.

(**A**)

(**B**)

Figure 11. An example of the attributes in the main station. (**A**) Attributes of the object; (**B**) Zoom-in the attributes in (**A**), where Symbol 1: manufacturer, symbol 2: type of power generation, Symbol 3: specification, Symbol 4: capacity, Symbol 5: diameter of fan, Symbol 6: weight.

Table 5. Illustrated issues from the videos.

Station	Illustrated Issues from the Videos
A	Operational procedure, substation, and power storage
B	Wind power and electricity transportation process
C	Construction of gravity-based foundations
D	Transportation of wind turbine tower and construction methods
E	Monopile foundation for offshore wind turbines (extension topic)

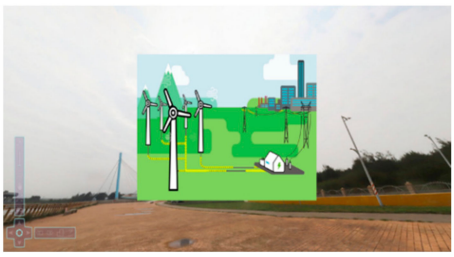

(**A**)

(**B**)

(**C**)

(**D**)

Figure 12. *Cont.*

(**E**)

Figure 12. Embedded videos in the same order as Table 5 for illustrating the issues related to wind farm knowledge. (**A**) Station A (video source from https://youtu.be/4Ha5vSlpW2w, accessed on 29 March 2022); (**B**) Station B (video source from https://youtu.be/DILJJwsFl3w, accessed on 29 March 2022); (**C**) Station C (video source from https://youtu.be/B4jEFPdUiMs, accessed on 29 March 2022); (**D**) Station D (video source from https://youtu.be/QK1hr_xCa_4, accessed on 29 March 2022); (**E**) Station E (video source from https://youtu.be/xKYClcExkMY, accessed on 29 March 2022).

4. Discussion

Developing the science and technology of geographic information with Cartography and Geomedia (including Multimedia) is one of the critical topics in the GIS domain. This direction demonstrates that applying different forms such as text, photography, images, animation, video, sound, music, virtual environment (e.g., 3D models), computer games, and others is useful for visualization or geovisualization [44]. These achievements presented in this study are highly correlated to the topics of interest (e.g., information potential of geomedia, geomedia for cartography, cartographic materials for construction and reconstruction in virtual space) in the special issue of Cartography and Geomedia. While comparing with the existing results for VR (e.g., Refs. [1–3]) and panorama (e.g., Refs. [22–24]) developments, our contributions not only constructed a virtual tour platform for the spatial and interactive visualization, but also explored the data quality with two major factors in multi-row panorama capturing (i.e., overlap rate and eccentric issue). Furthermore, visualizing the outside environment for onshore wind farms and the tourism site is rarely observed in the literature because of its complexity and specialization. Thus, readers can treat this article as one of the references for the development of cartography, geomedia, and geovisualization.

From a technical viewpoint in this study, an outdoor shoot can be influenced by various conditions. These factors make the displacement of the same target causing the stitching errors. More precisely, the SIFT algorithm cannot find the invariant location for the same target between different overlapped images. For example, image stitching requires identifying tie points between images; however, a moving photography subject may cause gaps or motion trails in the stitched image. In this study, the moving subjects include the clouds and wind turbine blades. Problems caused by cloud movement were resolved by setting the photography mode to the row-down setting and then slightly adjusting the images in Autopano. For problems caused by the rotation of turbine blades, images containing the blades were manually captured before using GigaPan for an automatic panoramic shoot (the same angle of view and instrument were used in the manual and automatic photography). In image stitching, images captured using GigaPan that contained blade rotation were replaced with the corresponding manually captured images to reduce incorrect tie point matching and thus increase the success rate of image stitching. Moreover, backlighting was a problem because the day of the shoot was sunny; thus, we took multiple shots at each station and rendered the images in Autopano to minimize chromatic aberration.

From the visualization and application-based perspective, the Street View function of Google Maps enables the public to explore popular tourist attractions; however, not all locations are covered by this function. The constructed platform for onshore wind

farms established in this study offers high-quality panoramas, detailed introductions to wind turbine functions, and videos illustrating wind turbine technology. This integration between panoramas and wind turbine introductions could expedite learning about wind power. From a tourist viewpoint, the information of provided attributes and videos is suitable for public users. From a civil engineering perspective, the installation and construction of wind turbines comprise various work stages, and a comprehensive plan is required to determine which methods, equipment, and machinery are used in accordance with the surrounding environment. For example, the turbine presented in Figure 11 has a diameter of 70.7 m, which requires a careful choice of crane and transportation tools for installation in accordance with the environment surrounding the construction site. The proposed platform provides opportunities for students and learners to practice making comprehensive construction plans. Therefore, this platform can be directly used to promote the tourism site and onshore wind farms, or be further extended for engineering education.

A wind turbine has an average useful life of 25 years and is operated and maintained by professionals. The Global Wind Organization has established a series of training standards for wind turbine maintenance technicians to foster the professional competence of the trainees. However, conducting intensive and large-scale physical training in an offshore wind farm is difficult. Therefore, panoramas of the internal structure of wind turbines could be incorporated into the proposed platform to familiarize maintenance technicians with the internal information, equipment, and related maintenance procedures of wind turbines. Additionally, wind turbines are constantly subject to lateral wind loads, which, when transferred to the pile foundation, cause it to undergo repeated axial tension or pressure, potentially resulting in the foundation structure tilting. A tilt angle of over 0.5° undermines the operational stability of a wind turbine [45]. Accordingly, fixed-point photography may be performed on a regular or irregular basis to document the tilt angle of wind turbines for subsequent engineering analyses.

5. Conclusions

Advancements in information technology (e.g., multimedia and cloud computing) and communication engineering (e.g., the establishment of 5G networks) have prompted new developments in tourism. People can now engage in realistic virtual travel experiences without being restricted by external factors (e.g., the COVID-19 pandemic, weather, or finances) and gain knowledge from these experiences. In this study, a multi-row panorama instrument and a single-lens reflex camera were used to capture images which were then stitched into panoramas. A multimedia-based travel platform was established with these panoramic images and equipped with interactive functions; the platform enables users to view panoramas in 360°. The stitching quality of panoramas was analyzed and improved to optimize the viewing experience.

The results reveal that the panorama image quality was affected by overlap rate, the relative position between the camera and GigaPan, brightness, and the number of identified tie points. Because the images were captured in an outdoor environment, weather was the primary factor directly affecting the photography result. Taking the shoot on a sunny, cloudless day could simplify the subsequent image processing tasks. Additionally, a higher overlap rate was associated with a lower RMSE and fewer stitching errors assuming that the camera was positioned appropriately. On average, the time required for the shoot doubled per 25% increase in overlap rate. Therefore, not only stitching quality but also the time required for shooting and subsequent image processing are key considerations. The optimal overlap rate should be selected according to the equipment performance and the purpose of these images to optimize outcomes. Panoramas were produced for six stations in this study; all of the stitching results had an average RMSE of less than five pixels. Wind power has been a focus of development in recent years in Taiwan; increasing attention has been paid to technological development and fostering talent in related fields. The proposed multimedia platform enables people confined to their homes to engage in travel experiences and to learn about wind turbines.

In summary, the contributions in this study not only take operations of multimedia production for spatial visualizations into consideration, but also test technical options with the overlap rate and the eccentric issue for improvement of data quality. The proposed framework can be also utilized to map the multi-row panoramic images for different users and cases. Future research could extend the applications of the platform to the internal structure of wind turbines or to offshore wind turbines to increase the diverse VR travel experiences on the platform and enhance public interest in wind turbines. On the other hand, the virtual-tour-based platform constructed by panoramic images in this study still provides the two-dimensional geometry causing that the accurate measurement is limited. Multiple panoramic stations for the photogrammetric task [46–49] to produce a truly 3D virtual tour can be explored in the future.

Author Contributions: Jhe-Syuan Lai and Chao-Ming Chi conceived and designed this study; Jhe-Syuan Lai, Yi-Hung Tsai and Min-Jhen Chang performed the experiments and analyzed the results; Jhe-Syuan Lai, Yi-Hung Tsai, Min-Jhen Chang, Jun-Yi Huang and Chao-Ming Chi wrote the paper. All authors have read and agreed to the published version of the manuscript.

Funding: This study was supported, in part, by (1) the Ministry of Education in Taiwan under the Project MOE-NEEMEC-B-108-02 for New Engineering Education Method Experiment and Construction, and (2) the Ministry of Science and Technology in Taiwan under the Projects 110-2221-E-035-029- and 109-2813-C-035-075-M.

Acknowledgments: The authors would like to thank (1) Fuan Tsai and Yu-Ching Liu in the Center for Space and Remote Sensing Research, National Central University, and (2) Ting-Yu Wu, Kuan-Lin Ho, Pei-Jun Su, and Ping-Tsung Chang in the Department of Civil Engineering, Feng Chia University, Taiwan, for supporting the software and panoramic instrument operation.

Conflicts of Interest: The authors declare that they have no conflicts of interest.

References

1. Oscar, A.; Eva, M.; Laura, C.; Alberto, P.; Diana, J. High-Fidelity Virtual objective structured clinical examinations with standardized patients in nursing students: An innovative proposal during the COVID-19 pandemic. *Healthcare* **2021**, *9*, 355.
2. Gao, Z.; Lee, J.; McDonough, D.; Albers, C. Virtual reality exercise as a coping strategy for health and wellness promotion in older adults during the COVID-19 pandemic. *J. Clin. Med.* **2020**, *9*, 1986. [CrossRef] [PubMed]
3. Van, N.; Vrana, V.; Duy, N.; Minh, D.; Dzung, P.; Mondal, S.; Das, S. The role of human–machine interactive devices for post-COVID-19 innovative sustainable tourism in Ho Chi Minh City, Vietnam. *Sustainability* **2020**, *12*, 9523. [CrossRef]
4. Graabak, I.; Korpås, M. Variability characteristics of European wind and solar power resources—A review. *Energies* **2016**, *9*, 449. [CrossRef]
5. Thayumanavan, P.; Kaliyaperumal, D.; Subramaniam, U.; Bhaskar, M.; Padmanaban, S.; Leonowicz, Z.; Mitolo, M. Combined harmonic reduction and DC voltage regulation of a single DC source five-level multilevel inverter for wind electric system. *Electronics* **2020**, *9*, 979. [CrossRef]
6. Ganea, D.; Amortila, V.; Mereuta, E.; Rusu, E. A joint evaluation of the wind and wave energy resources close to the Greek Islands. *Sustainability* **2017**, *9*, 1025. [CrossRef]
7. Feng, T.; Yang, Y.; Yang, Y.; Wang, D. Application status and problem investigation of distributed generation in China: The case of natural gas, solar and wind resources. *Sustainability* **2017**, *9*, 1022. [CrossRef]
8. Chang, C. Wind Power Generation Prediction Using Data Mining Technique: The Case of Chang Kung Wind Farm. Master's Thesis, National Chung Hsing University, Taichung, Taiwan, 2018.
9. Cheng, K.-S.; Ho, C.-Y.; Teng, J.-H. Wind and see breeze characteristics for the offshore wind farms in the central coastal area of Taiwan. *Energies* **2022**, *15*, 992. [CrossRef]
10. 4C Offshore. Available online: https://www.4coffshore.com/windfarms/windspeeds.aspx (accessed on 8 April 2022).
11. Burdea, G. Virtual reality systems and applications. In Proceedings of the Electro/93 International Conference, Short Course, Edison, NJ, USA, 28 April 1993.
12. Weng, C. A Study on Sense of Space and Presence in Virtual Space. Ph.D. Thesis, National Chiao Tung University, Hsinchu, Taiwan, 2007.
13. Bricken, M. Virtual reality learning environments: Potentials and challenges. *Comput. Graph.* **1991**, *25*, 178–184. [CrossRef]
14. Michitaka, H. Virtual reality technology and museum exhibit. *Int. J. Virtual Real.* **2006**, *5*, 31–36.
15. Lai, J.; Peng, Y.; Chang, M.; Huang, J. Panoramic mapping with information technologies for supporting engineering education: A preliminary exploration. *ISPRS Int. J. Geo-Inf.* **2020**, *9*, 689. [CrossRef]
16. Soliman, M.; Pesyridis, A.; Dalaymani-Zad, D.; Gronfula, M.; Kourmpetis, M. The application of virtual reality in engineering education. *Appl. Sci.* **2021**, *11*, 2879. [CrossRef]

17. FernandoJ, F.; Rebeca, M.; Manuel, C. Constructionist learning tool for acquiring skills in understanding standardised engineering drawings of mechanical assemblies in mobile devices. *Sustainability* **2021**, *13*, 3305.
18. Lee, H.; Lee, J. The effect of elementary school soccer instruction using virtual reality technologies on students' attitudes toward physical education and flow in class. *Sustainability* **2021**, *13*, 3240. [CrossRef]
19. Louvre. Available online: https://www.louvre.fr/en/visites-en-ligne (accessed on 29 March 2022).
20. Great Wall of China. Available online: https://www.thechinaguide.com/destination/great-wall-of-china (accessed on 29 March 2022).
21. Lee, C. Applying Orient-Object Technique to Construct 3D Virtual Tourism—A Case Study in the Yeliou Geo-Park. Master's Thesis, National Taiwan University, Taipei, Taiwan, 2007.
22. Harrington, M.; Bledsoe, Z.; Jones, C.; Miller, J.; Pring, T. Designing a virtual arboretum as an immersive, multimodal, interactive, data visualization virtual field trip. *Multimodal Technol. Interact.* **2021**, *5*, 18. [CrossRef]
23. Antonio, M.; Alberto, R.; Gasparini, M.; Hornero, A.; Iraci, B.; Martín-Talaverano, R.; Moreno-Escribano, J.; Muñoz-Cádiz, J.; Murillo-Fragero, J.; Obregón-Romero, R.; et al. A heritage science workflow to preserve and narrate a rural archeological landscape using virtual reality: The Cerro del Castillo of Belmez and its surrounding environment (Cordoba, Spain). *Appl. Sci.* **2020**, *10*, 8659.
24. Mariotto, F.; Bonali, F. Virtual geosites as innovative tools for geoheritage popularization: A case study from eastern Iceland. *Geosciences* **2021**, *11*, 149. [CrossRef]
25. Garinko Ice-Breaker Cruise 360 Experiences. Available online: https://www.youtube.com/watch?v=W3OWKEtVtUY (accessed on 29 March 2022).
26. Chao, T.-F. The Study of Virtual Reality Application in Education Learning—An Example on VR Scientific Experiment. Master's Thesis, National Kaohsiung First University of Science and Technology, Kaohsiung, Taiwan, 2009.
27. Li, Y.; Song, H.; Guo, R. A study on the causal process of virtual reality tourism and its attributes in terms of their effects on subjective well-being during COVID-19. *Int. J. Environ. Res. Public Health* **2021**, *18*, 1019. [CrossRef]
28. Chiao, H.-M.; Chen, Y.-L.; Huang, W.-H. Examining the usability of an online virtual tour-guiding platform for cultural tourism education. *J. Hosp. Leis. Sport Tour. Educ.* **2018**, *23*, 29–38. [CrossRef]
29. Panos. Available online: https://www.panosensing.com.tw/faq6/ (accessed on 29 March 2022).
30. Ernie, H.; Mark, K. Implementing GigaPan technology into an airport's foreign object debris management program. *Transp. Res. Rec. J. Transp. Res. Board* **2013**, *2336*, 55–62.
31. Zheng, J.; Zhang, Z.; Tao, Q.; Shen, K.; Wang, Y. An accurate multi-row panorama generation using multi-point joint stitching. *IEEE Access* **2018**, *6*, 27827–27839. [CrossRef]
32. Liu, X.C.; Guo, X.T.; Zhao, D.H.; Cao, H.L.; Tang, J.; Wang, C.G.; Shen, C.; Liu, J. Integrated velocity measurement algorithm based on optical flow and scale-invariant feature transform. *IEEE Access* **2019**, *7*, 153338–153348. [CrossRef]
33. Lyu, W.; Zhou, Z.; Chen, L.; Zhou, Y. A survey on image and video stitching. *Virtual Real. Intell. Hardwar* **2019**, *1*, 55–83. [CrossRef]
34. Lee, H.; Lee, S.; Choi, O. Improved method on image stitching based on optical flow algorithm. *Int. J. Eng. Bus. Manag.* **2020**, *12*, 1–17. [CrossRef]
35. Lee, Y.A. Comparative Analysis on the Traditional and Digital Interface of Single-Lens Reflex Cameras—A Case Study of Exposure Control. Master's Thesis, National Taiwan University of Science and Technology, Taipei, Taiwan, 2009.
36. Cooper, J.D.; Abbott, J.C. *Exposure Control and Lighting (Nikon Handbook)*; Amphoto: Kansas, MI, USA, 1979.
37. Lowe, D.G. Object recognition from local scale-invariant features. In Proceedings of the 7th IEEE International Conference on Computer Vision, Kerkyra, Greece, 20–29 September 1999.
38. Wang, G.; Wu, Q.M.J.; Zhang, W. Kruppa equation based camera calibration from homography induced by remote plane. *Pattern Recogn. Lett.* **2008**, *29*, 2137–2144. [CrossRef]
39. Sakharkar, V.S.; Gupta, S.R. Image stitching techniques—An overview. *Int. J. Comput. Sci. Appl.* **2013**, *6*, 324–330.
40. Blending in AutoPano Video Pro. Available online: https://www.youtube.com/watch?v=knqT-2UJOao (accessed on 29 March 2022).
41. What Is Blending? Autopano Video Pro. Available online: https://www.youtube.com/watch?v=H6Tjq0rB9UA (accessed on 29 March 2022).
42. Zeng, B.; Huang, Q.; Saddik, A.E.; Li, H.; Jiang, S.; Fan, X. Advances in multimedia information processing. In Proceedings of the 19th Pacific-Rim Conference on Multimedia, Hefei, China, 21–22 September 2018.
43. Koehl, M.; Brigand, N. Combination of virtual tours, 3D model and digital data in a 3D archaeological knowledge and information system. In Proceedings of the XXII ISPRS Congress, Melbourne, Australia, 25 August–1 September 2012.
44. Medynska-Gulij, G.; Forrest, D.; Cybulski, P. Modern cartographic forms of expression: The renaissance of multimedia cartography. *ISPRS Int. J. Geo-Inf.* **2021**, *10*, 484. [CrossRef]
45. Huang, T.-Y. Deformation Responses of Piles in Cohesionless Soil under Cyclic Axial Tension Loads. Master's Thesis, National Cheng Kung University, Tainan, Taiwan, 2014.
46. Lee, I.-C.; Tsai, F. Applications of panoramic images: From 720° panorama to inerior 3D models of augmented reality. In Proceedings of the Indoor-Outdoor Seamless Modelling, Mapping and Navigation, Tokyo, Japan, 21–22 May 2015.
47. Tsai, V.J.D.; Chang, C.-T. Three-dimensional positioning from Google street view panoramas. *IET Image Process.* **2013**, *7*, 229–239. [CrossRef]
48. Huang, T.-C.; Tseng, Y.-H. Indoor positioning and navigation based on control spherical panoramic images. *J. Photogram. Remote Sens.* **2017**, *22*, 105–115.
49. Teo, T.-A.; Chang, C.-Y. The generation of 3D point clouds from spherical and cylindrical panorama images. *J. Photogram. Remote Sens.* **2018**, *23*, 273–284.